Measurement of ionization rates of Ti IX, Ne VI, Ne VII, and O VI

R. U. Datla* and J. R. Roberts
National Bureau of Standards, Washington, D.C. 20234
(Received 6 June 1983)

The effective ionization rates of Ti IX, Ne VI, Ne VII, and O VI have been measured with the use of the plasma spectroscopy method in a θ pinch discharge at an electron temperature (50—60 eV) much below their ionization threshold and at an electron density of $(\simeq 2-3)\times 10^{16}$ cm^{-3}. A theoretical analysis of the effective ionization rates showed that excitation ionization is a major contributing process. Theoretical values are in reasonable agreement with experiment.

I. INTRODUCTION

Many papers[1–7] have been published over the past two decades reporting the measurements of effective ionization rates of various ions using the plasma spectroscopy method with θ pinches. Basically, in this method, the time histories of emission line intensities from impurity ions of interest are observed from the laboratory plasma by means of a spectrometer-photomultiplier. The plasma electron temperature and electron density are measured. With the use of these two parameters as input to the time-dependent corona model for ionic populations and corona model for excitation equilibrium, the time histories of emission line intensities are predicted. In order to have a realistic temperature dependence of the ionization rates in the computer model the analytical formulation of Lotz[8] is used. The specific equation used is given in Ref. 2. This equation is hereafter called the Lotz-Kunze semiempirical formula. The simulation is carried out iteratively on a computer by varying a multiplicative constant of the ionization rates, to find the predicted line intensity time histories that best match the experimental ones. This method gives the total ionization rate which is the sum of all effective processes such as electron impact ionization from the ground state, excited states, and inner shells. There have been agreements and disagreements[3] between theoretical predictions and experimental values and there is a constant need to increase the experimental data base to clearly understand the various contributing processes. We selected ions of different elements with similar ionization potentials, but different atomic structures to cross check the consistency of our experimental results.

In Sec. II we describe the principles of measurements, experimental arrangement, diagnostics of the plasma condition, and the measurement of ionization rates. In Sec. III we make theoretical predictions of the total ionization rates and compare them with experiment. The results show that, at the electron temperatures and densities of the present experiment, the multiple step process of excitation-ionization makes significant contributions to the total rate.

II. EXPERIMENT

A. Spectroscopy method

The present experiment is carried out on the 50-kJ θ pinch at the National Bureau of Standards[5] (NBS). The assumptions and limitations imposed by the plasma spectroscopy method for experimental conditions in a θ pinch plasma are summarized in Ref. 6. In order that the plasma spectroscopy method be applicable, the time histories of emission line intensities should be more sensitive to the ionization rates than to variations in electron density, electron temperature, and plasma length. In general, a quiescent time frame exists in a θ pinch plasma between the time of initial rapid compression and the time the plasma drifts to the wall and/or end losses become important. During this time frame the plasma spectroscopy method is valid. However, such a time frame can only be established by diagnosing the plasma thoroughly using various techniques. As noted in Ref. 6, it helps to operate the θ pinch with a small reversed bias field to avoid axial inhomogeneities and obtain better confinement. Finally, observation of identical time histories for the emission line intensities along the radial and longitudinal directions of the plasma gives a good indication of the quiescent time frame.

B. Experimental arrangement

The details of the NBS θ pinch are described in Ref. 5. Only the differences are noted here. The preheater bank was charged to -12.5 kV and had a ringing period of 2.8 μsec. Preionizer and bias banks were charged to 30 and 2 kV, respectively, and were fired at the same time. The preheater was fired after a 5 μsec delay. The main bank was charged to -18 kV and was fired after a 25 μsec delay. For the purpose of this experiment, the quartz discharge tube was filled with 30 mTorr H_2 and 0.3 mTorr Ne. Oxygen is an ambient impurity in the discharge tube. Titanium was injected as an impurity by using a coaxial gun discharge with titanium electrodes. The coaxial gun consisted of a 2-cm-diam, 0.5-cm-thick, and 3.2-cm-long annular cylinder as one electrode, with a center rod of the same length and 0.5 cm diameter as the other electrode. The center rod was welded to the center pin of an automotive spark plug, with the threaded annular electrode screwed to the spark plug threads. The spark plug served as the insulator between the electrodes and as the vacuum interface. A single 8.6-μF capacitor at 16 kV was discharged to fire the gun plasma. The period of the discharge was 20 μsec. The gun plasma containing Ti was found to expand and travel away from the electrodes. The gun was located at one end of the discharge tube, 60 cm

away from the center of the coil. It was offset from the axis of the discharge tube so that a blue glass could be held on top of the outer electrode at a Brewster angle to serve as a beam dump for the ruby laser that is used to measure electron density and temperature by 90° Thomson scattering.

The amount of Ti impurity injected into the θ pinch plasma was studied by firing the preheater bank only. The intensities of Ti II lines grouped at 3760 Å were observed at the coil center perpendicular to the θ pinch axis, varying the time delay between the firing of the gun discharge and the preheater discharge. The bulk of Ti atoms were found to arrive at the observation point with a speed of one centimeter per μsec, followed by a constant stream of atoms at a lower density traveling at approximately half that speed. Observation of Ti II line intensities from the tip of the electrodes showed that the gun plasma was formed only during the first two half-cycles of the current ringing. In this experiment, we used the lower density part of the injected Ti from the gun, so the conditions would be changed the least. Spectral lines from O VI, Ne VI, Ne VII, and Ne VIII were monitored end-on by using a 2.2-m grazing-incidence monochromator below 500 Å and a 0.25-m spectrometer for lines above 2000 Å. The time delay between the firing of the gun discharge and the θ pinch discharge was empirically adjusted so that no differences were found in the monitored time histories of the lines from ions mentioned earlier. A factor of 2 variation in the absolute intensities of spectral lines from Ti ions due to the shot-to-shot variation of the gun performance did not change the plasma condition as indicated by the monitors. This is because we have a very small amount of Ti in the plasma. Periodic cleaning of electrodes or reinstallation of a new plasma gun was necessary every 60—70 shots to maintain a reasonably reproducible Ti concentration. The most critical parameter that influenced the gun performance was its voltage of operation. At voltages below 10 kV, the gun would misfire and at voltages above 18 kV, the spark plug would not hold off the voltages or the electrodes would quickly deteriorate. The optimum voltage for the gun was found to be 16 kV.

C. Diagnostics

End-on framing pictures. The gross dynamics of the plasma behavior were studied by utilizing a high-speed framing camera. End-on pictures were taken at 200-nsec intervals with 100-nsec integration times. Figure 1 shows some of the framing pictures and demonstrates that the plasma compression is uniform. The time between 2.0 and 3.0 μsec was the quiescent time frame even though radial "flute" instabilities were seen in some shots (Fig. 1). The plasma steadily drifted towards the collector plate, and at 3.2 μsec after the initiation of main bank discharge the plasma hit the wall at the collector plate side and showed an increase of visible light emission (Fig. 1). However, the plasma was found to be totally within the field of view of the grazing incidence spectrograph between 2.0 and 3.0 μsec.

Visible and uv spectroscopy. Emission line time histories of N V and O VI were obtained, with two 0.25-m spectrometers viewing, end-on along the θ pinch axis and side-on at the midplane of the coil. The side-on time history of an emission line from an ion that occurred during the implosion phase, e.g., N V, showed its peak emission occurring 0.2 μsec earlier than its end-on observation. This is attributed to the spatial inhomogeneity at those early times, arising from the imploding annular plasma. However, ions occurring after implosion, e.g., O VI, had identical time histories observed side-on or end-on, indicating a homogeneous plasma from the time of occurrence of O VI. The end-on time histories of lines from C IV, N V, and O VI peaked at 1.0, 1.5, and 2.2 μsec, respectively, after the initiation of the main bank discharge. The side-on observations were reproducible at various longitudinal locations viewed through holes in the coil. O VI line emission occurred along the entire length of the coil, i.e., 40 cm. However, the line intensity was uniform only over the middle 27 cm and it fell in value outside this region up to the coil ends. The length of the plasma is thus considered to be 27 cm.

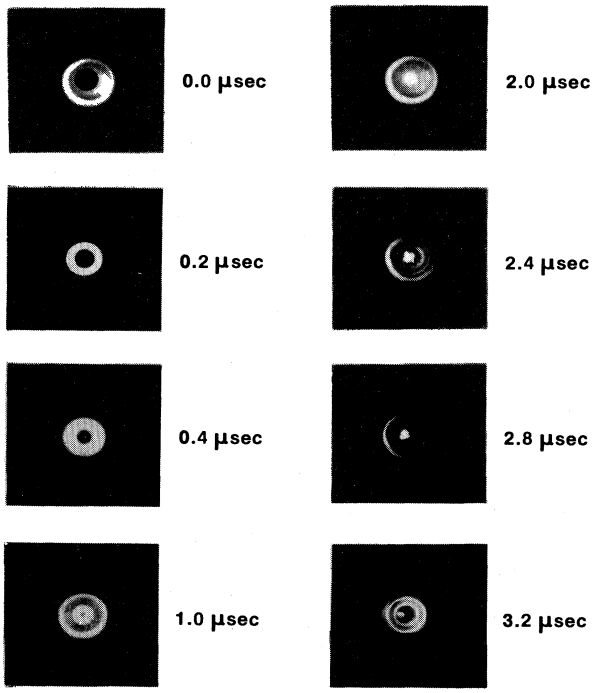

FIG. 1. End-on framing pictures of the θ pinch plasma. Time delay of each frame from the initiation of the main bank discharge is stated. Each frame is of 100-nsec duration.

The implosion phase was further studied by the following procedure, to ascertain whether the central core of the plasma is heated along with the imploding ring. A 2.25-m spectrograph with an optical multichannel analyzer (OMA) at the exit plane viewed the plasma side-on at the midplane of the coil. The $3s$-$3p$ transition lines from C IV (5.801.5 Å), N V (4603.8 and 4619.9 Å), and O VI (3811.4 and 3834.2 Å) were observed. The OMA was electronically gated to observe each transition for its total time of occurrence. The observations of lines from N V and O VI ions are shown in Figs. 2(a) and 2(b), respectively. Two

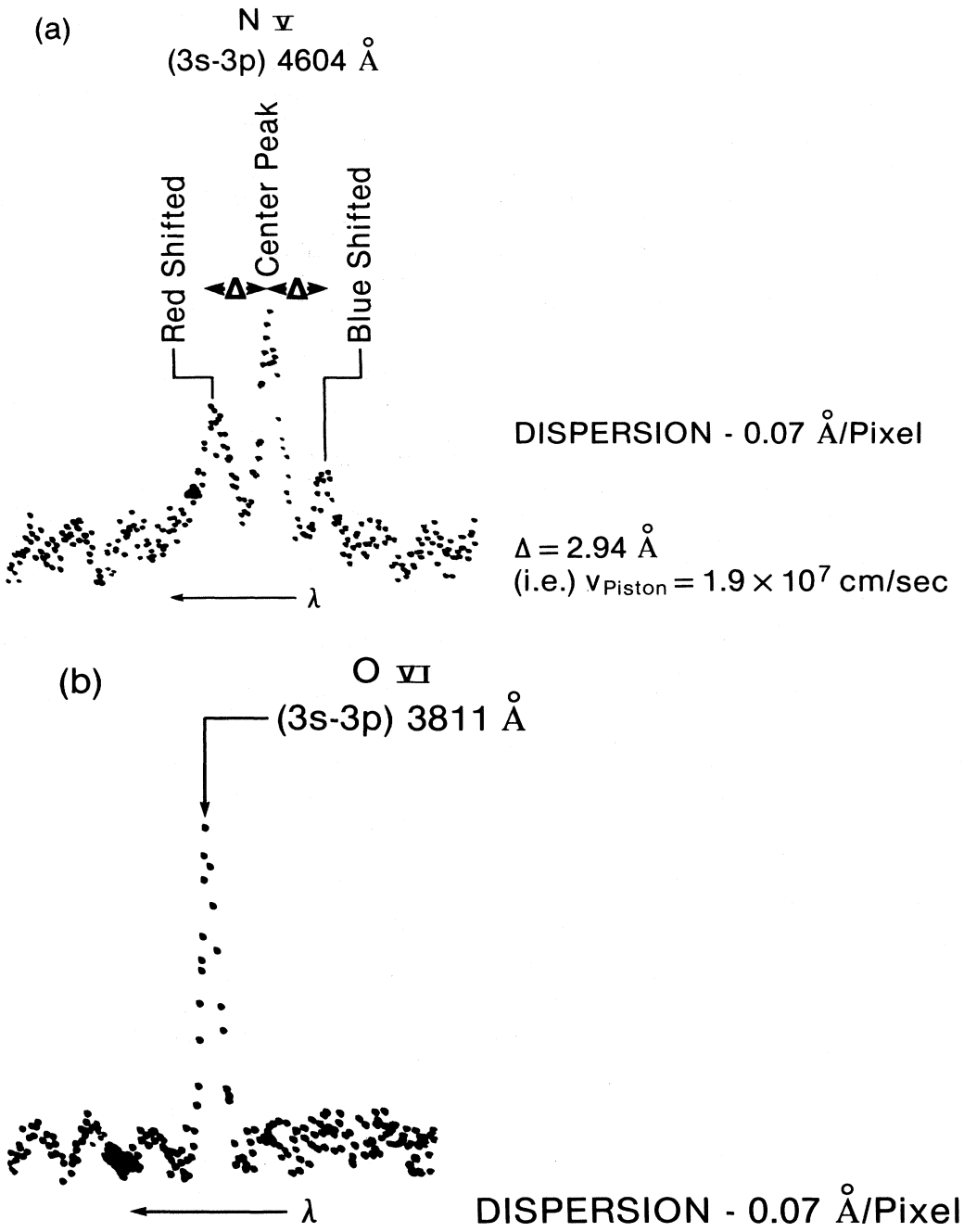

FIG. 2. Side-on observation of a $3s$-$3p$ transition in (a) N V and (b) O VI with a 2.25-m Ebert spectrograph equipped with an OMA at the exit plane. Dispersion is given in units of Å/pixel (picture element).

Doppler-shifted components, one shifted to the red, the other shifted to the blue symmetrically situated on either side of the unshifted peak of the line position, were observed for lines from C IV and N V [shown in Fig. 2(a)]. The possible reason for the lower intensity of the blue-shifted component is discussed in the next section. The unshifted line component is emitted from the central core whereas the other two are Doppler-shifted peaks caused by the imploding piston observed side-on. This kind of observation on the θ pinch implosion and its explanation is well documented in the literature.[9,10] However, O VI lines which peak at 2.2 μsec had only the central peak, but no side components [Fig. 2(b)]. These observations confirmed that the central core of the plasma is continually heated and the directed velocities in the implosion are all randomized by the time of the occurrence of O VI. Ion temperatures of 50 eV for N V and 70 eV for O VI were deduced from the Doppler widths of their lines. The piston

velocity deduced from the Doppler shifts in Fig. 2(a) is 1.9×10^7 cm/sec.

Thomson scattering. The light from a 5-J ruby laser is focused, parallel to the axis of the discharge tube, to a 1.5-mm spot in the plasma. The scattered light was observed at 90° through the center hole in the main coil with a 0.3-m Czerny-Turner monochromator equipped with a five-channel glass fiber-optic photomultiplier system. The channels were calibrated relative to each other by using a tungsten strip lamp. Rayleigh scattering from N_2 is used to absolutely calibrate the detection system in order to measure the electron density. The laser and the scattering detection system are mounted on a table movable parallel and perpendicular to the discharge tube to make local measurements of electron density and electron temperature anywhere in the plasma. The experimental light-scattering intensity profile as a function of wavelength agreed very well with the scattering profile expected from a Maxwellian velocity distribution of electrons. Figures 3(a) and 3(b) show the average electron density and electron temperature, respectively, obtained by averaging the local measurements of these plasma parameters at 2-mm intervals along the diameter at the midplane of the coil. Owing to high background of plasma bremsstrahlung during the implosion and low electron temperature no data could be obtained prior to 1.5 μsec from the initiation of the main bank discharge. The error bars shown in Fig. 3 are one standard deviation of the mean. Individual local measurements were repeated at least three times. The radial profile of the plasma has a dip in density and a peak in temperature over a (5—10)-mm region around the center of a 2-cm-diam plasma. The radial scan also revealed that during the quiescent time interval from 2.0 to 3.0 μsec the plasma is undergoing adiabatic compression with the bias field trapped in the middle. However, the electron density on the collector plate side was lower than on its opposite side. It is attributed to the asymmetry in the compressing field caused by the gap in the coil at the interface of the coil and the collector plate. The lower electron density in that part of the annulus moving towards the spectrometer during the implosion makes the blue-shifted component weaker in intensity than the red-shifted component as described in the preceding section [Fig. 2(a)]. In fact, this asymmetry causes the plasma drift to the wall on the collector plate side. The scattering measurements were thus irreproducible from shot to shot for times beyond 3.0 μsec.

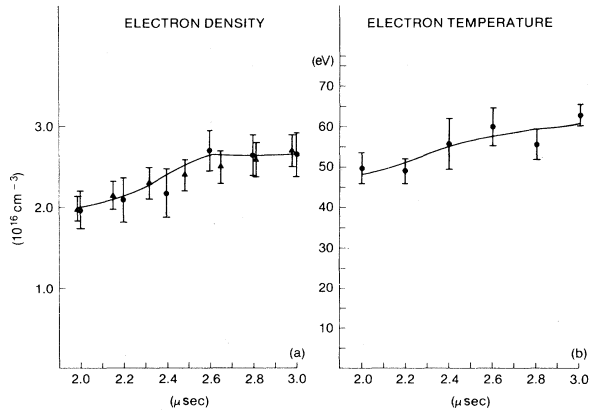

FIG. 3. (a) Radial average electron density (——) as a function of time. Dotted points (●) are obtained by Thomson scattering using a ruby laser. Triangular (▲) points are obtained by He-Ne—laser interferometer. (b) Radial average electron temperature (——) as a function of time obtained by Thomson scattering using a ruby laser.

The observed plasma motion in the scattering measurements was consistent with end-on framing pictures. The Thomson scattering measurements were also done along the axis at different locations where there are holes in the coil and the measured plasma parameters were within error limits shown in Fig. 3. No detailed temporal and radial scan at each axial position was done because of the prohibitively large amount of work involved.

Laser interferometry. A He-Ne—laser interferometer was set up end-on to obtain the line average plasma electron density. The experimental arrangement is described in Ref. 11. Signals proportional to the sine and cosine of the phase shift of the laser light due to the refractive index changes in the plasma were digitized continuously at 25-nsec intervals, and were analyzed by a computer. The laser beam diameter was ~5 mm and the plasma was scanned radially shot by shot along the diameter at 5-mm intervals. The line average electron density was deduced using the measured plasma length discussed earlier. The points marked with triangles in Fig. 3(a) show the average electron density observed during the time frame of 2.0—3.0 μsec from the initiation of the main bank. The bars indicate the standard deviation of the mean. The agreement between the interferometer results and the laser scattering results is very good.

D. Ionization rates

The time histories of emission lines from Ne VI, Ne VII, Ne VIII, Ti IX, Ti X, Ti XI, O V, and O VI were observed end-on with a 2.2-m grazing-incidence spectrometer equipped with a 1800-lines/mm holographic grating. A 1-m grazing-incidence spectrometer with a 1200-lines/mm grating was also used end-on and the two spectrometers viewed the plasma from opposite ends. Identical time histories were observed by both spectrometers. At least three transitions with different Δn values were observed from each ion. Lines from each ion were found to have identical time histories. Ions occurring earlier in the dynamic phase of the implosion, e.g., Ne V, Ti VIII, were found to have weak emission lines that varied widely from shot to shot. Also, lines from Ti X and Ti XI did not show consistent time histories from shot to shot. It is presumed that they never reached their peak intensities during the quiescent phase of the plasma. The continuous lines in Figs. 4(a)—4(c) show the intensity variations of the emission lines as a function of time from the initiation of the main bank discharge. The horizontal bars indicate the maximum variation from shot to shot in each ionic line time history.

A computer simulation of the time histories of the observed spectral lines is accomplished in the following way.

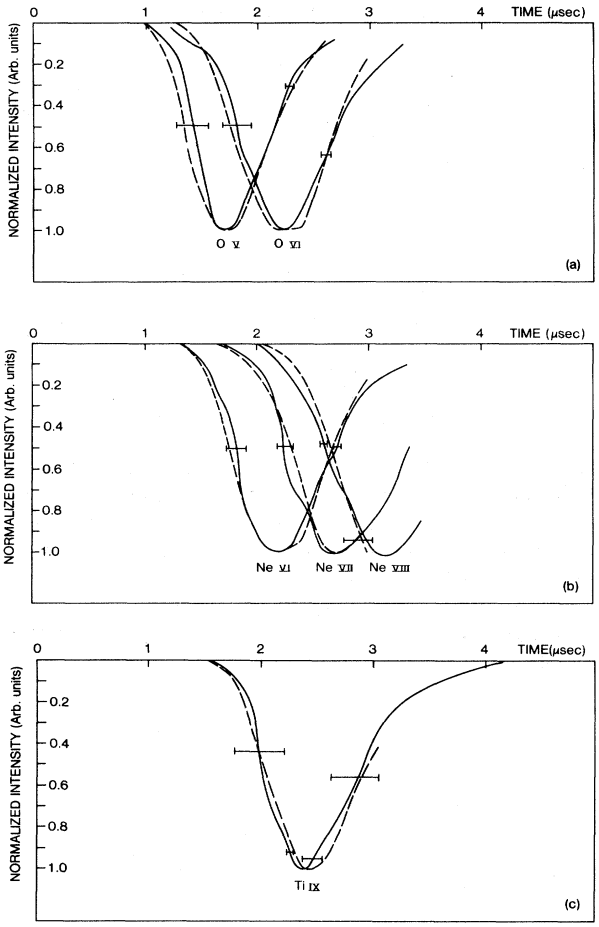

FIG. 4. Intensities of emission lines normalized to their peak values as a function of time from the initiation of the main bank. Experiment (——); theoretical simulation (— — —). (a) O V and O VI (ionization potentials 113.9 and 138.2 eV); (b) Ne VI, Ne VII, and Ne VIII (ionization potentials 157.9, 207.3, and 239.1 eV); (c) Ti IX (ionization potential 193.0 eV).

The average electron density and electron temperature profiles, shown in Fig. 3, and the appropriate atomic data, such as ionization energies, are used as input data for solving the coupled set of rate equations. The time-dependent ion populations that result from this simulation are then used to calculate specific spectral line intensities utilizing the corona model for level populations within an ion and the temperature dependence of the Gaunt factor approximation[12] for the excitation rates. As noted earlier, the experimental determination of the initial ion distribution is a formidable task due to the inhomogeneity of the plasma undergoing its rapid compression. Thus fictitious ionization rates are chosen for low-Z ions up to the quiescent phase. For the ionic states occurring in the quiescent phase, the computer simulation is iterated by varying multiplicative constants of the ionization rates as given by the Lotz-Kunze semiempirical formula. This is done until a proper match of the computed time histories with the experimental ones is found. The dashed lines drawn in Figs. 4(a)—4(c) show these simulated time histories in comparison to the experimental ones. The ionization rates thus determined are given in the last column of Table II at a specific plasma temperature and density of the present experimental conditions.

III. THEORETICAL COMPARISON

The ground-state ionization rates calculated by using various theoretical approaches excluding inner-shell effects are given in Table I. They are the semiempirical values predicted by Lotz and the theoretical calculations of the following: Younger[13,14] using a distorted-wave approach (Y); Golden and Sampson[15,16] using the $Z=\infty$ method (GS); Summers[17] using the semiclassical approach (ECIP) introduced by Burgess.[18] The semiempirical values of Lotz essentially agree with the calculations of Younger and Golden and Sampson, whereas they are a factor of 2 higher than the ECIP values.

The present experimental effective ionization rates are compared with theory in Table II. Column 2 gives the values calculated by using the Lotz-Kunze semiempirical formula including the inner shells. The ionization rates from levels close to the ground state that are metastable, or where the transition probability for a spontaneous emission is comparable to the excitation rate, is given in column 3. These levels, e.g., the $2p$ level in O VI, the $2s\,2p^2(^4P)$ levels in Ne VI, the $2s\,2p(^3P)$ levels in Ne VII, the $3s^2 3p^2$ singlets and $3s\,3p^3$ triplets in Ti IX, are considered as populated according to the Boltzmann factors with respect to the ground state, due to the high electron density in our experiments. This should be considered only as an upper limit, as the importance of radiative decay compared to collisional excitations may lower these populations.

The following theoretical consideration is given to indicate the contribution of highly excited states in each ion to

TABLE I. Calculated ground-state ionization-rate coefficients (in units of 10^{-11} cm^3 sec^{-1}) at an electron temperature of 55 eV.

ion	$\frac{kT^a}{E}$	Lotz-Kunze	Y	GS	ECIP
Ti IX	0.28	2.62		2.98	1.12
Ne VI	0.35	3.59		4.03	1.87
Ne VII	0.27	1.78	1.70	1.77	1.0
O VI	0.40	6.63	6.07	6.01	3.37

[a] kT is the electron temperature and E is the ionization potential.

TABLE II. Effective ionization rates (in units of 10^{-11} cm^3/sec) at an electron temperature of 55 eV and an electron density of 2.5×10^{16} cm^{-3}.

Ion	Estimated contributions to the total effective ionization rate using the Lotz-Kunze semiempirical formula				S_{eff} total		S_{eff} (expt.)
	Ground state including subshells	Low-lying levels or metastable levels including subshells	Excited states above collision limit		Method 1	Method 2	
			Method 1	Method 2			
(1)	(2)	(3)	(4)	(5)	(6)	(7)	(8)
Ti IX	3.63	0.98	1.71	4.5	6.32	9.11	9.4
Ne VI	6.91	1.11	2.25	1.99	10.27	10.01	10.8
Ne VII	1.78	0.32	0.59	0.82	2.69	2.92	3.8
O VI	6.63	2.19	2.46	2.92	11.28	11.74	14.0

the total effective ionization rate at the high electron density and low electron temperature of our experiment. The radiative decay rate from highly excited states in an ion decreases with increasing principal quantum number in the hydrogenic approximation. In contrast, the rate of collisional excitation to higher excited levels increases because of the decreasing energy difference between levels. Therefore, one can define a collision limit[20] n' as the lowest principal quantum number for which further collisional excitation is as probable as radiative decay. Thus, for excited states above n' ionization would be more likely by further collisions.

The collision limit n' is determined for each ion in the hydrogenic approximation using the following expression given in Ref. 20:

$$n'=1.26\times10^2Z^{14/17}N_e^{-2/17}\left[\frac{kT}{Z^2E_H}\right]^{1/17}\times\exp\left[\frac{4Z^2E_H}{17n'^3kT}\right], \quad (1)$$

where Z is the number of effective charges ($Z=6$ for O VI), N_e is the electron density and kT is the electron temperature. n' is 6 for O VI, Ne VI, and Ne VII, and 7 for Ti IX in our experiment. The contribution of excited states above the collision limit to the effective ionization rate is estimated for each ion by following two different procedures and is given in columns 4 and 5 in Table II under the titles of method 1 and method 2, respectively. In method 1, we used the following expression derived from equations 6-90 and 6-91 of Ref. 20, to obtain this contribution as a fraction of the direct ionization:

$$\frac{S_{\text{excitation-ionization}}}{S_{\text{direct ionization}}}=\exp\left[\frac{Z^2E_H}{n'^2kT}\right]-1. \quad (2)$$

This fractional contribution was 28% for O VI, Ne VI, and Ne VII and 37% for Ti IX. These percentages are converted into rates by multiplying the direct ionization rates as given in columns 2 and 3, and their sums are given in column 4. The sums of the rates in columns 2, 3, and 4 are given in column 6.

In method 2, we calculated the ionization rates by the Lotz-Kunze semiempirical formula with the ionization potentials lowered to the collision limit energy.[4,15] The sums of these rates are given in column 7. Therefore, the contribution due to excitation-ionization given in column 5 is the difference between these rates and the sum of the rates given in columns 2 and 3. In Ref. 4, this method gave 25% correction to the experimental rate to arrive at the ground-state ionization rate of Li-like ions. Both methods give values in reasonable agreement for O VI and Ne VI whereas they differ for Ne VII and Ti IX. In any

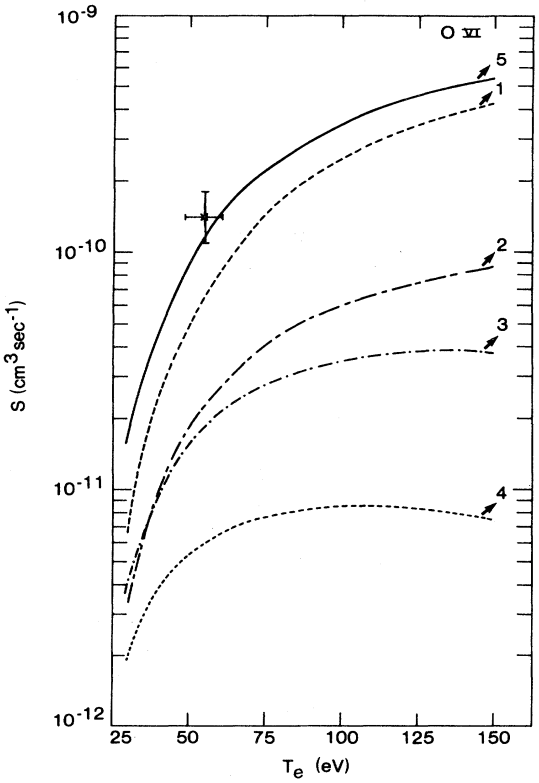

FIG. 5. Various components and the total O VI ionization rate as a function of electron temperature at an electron density of 2.5×10^{16} cm^{-3}. Ionization from the $2s$ level (1), from the $2p$ level (2). Excitation-ionization from $2s$ level (3), excitation-ionization from the $2p$ level (4). Total rate (5) and the result of this experiment ($\times$).

case the values given in columns 4 and 5 are only indicative of the important contribution due to excitation-ionization. The theoretical rates given in columns 6 and 7 are reasonably close to the experimental values given in column 8. However, if we compare the contributions of the ground state including inner-shell parts only, the experimental rates are a factor of about 2 higher than theory.

Experimental errors for the measured ionization rates are estimated to be $\pm 20\%$ for O VI, $\pm 30\%$ for Ne VI and Ne VII, and $\pm 40\%$ for Ti IX. The error arises from the experimental uncertainties in the time histories of emission lines and the electron density. The estimated uncertainty in our electron temperature measurement is $\pm 10\%$. To illustrate this graphically, the measured ionization rate of O VI with error limits and the estimated contributions from various processes as a function of electron temperature are shown in Fig. 5 for an electron density of 2.5×10^{16} cm^{-3}. In this figure, curves 1, 2, 3, and 4 are the ionization rate contributions from the $2s$ level, the $2p$ level, excitation-ionization from the $2s$ level (method 1) and excitation-ionization from the $2p$ level (method 1), respectively. The total ionization rate is shown by the curve labeled 5. The experimental value is close to the expected total rate based on the Lotz-Kunze semiempirical formula.

The contribution to total ionization by the ionization from the triplet metastable levels in He-like and Be-like ions and the $2p$ level in Li-like ions have been accounted for first in earlier experiments in Refs. 1 and 2, respectively. Also, the possibility of excitation-ionization processes involving levels above the collision limit substantially modifying the ground-state ionization rate was mentioned by Lotz in Ref. 19. While only a very approximate estimation of contributions from excited states is done here, we find the multiple-step process of excitation-ionization to be very important since it may contribute as much as direct ionization, especially at temperatures where the exponential term in Eq. (2) is much larger than one. This process could account for the disagreement with theory in experiments done at electron temperatures below threshold for direct ionization.[5]

The following discrepancies between theory and experiment reported in the literature are yet to be resolved. The ionization rates deduced from measured cross sections[21] of O VI and N V agree with the predictions of Lotz-Kunze while they disagree for C IV. The measured ionization rates[2,3,6] using θ pinches at temperatures close to and above threshold agree well with theory for H-like and He-like ions whereas they are 35—50% below the Lotz-Kunze predictions for Li-like and other high-Z ions. It should be noted that the measured ionization rates of O VI and N V of Ref. 4 agreed with Lotz-Kunze predictions at a temperature close to threshold after accounting for excitation-ionization processes.

The process of excitation-autoionization[21,22] is neglected in our analysis because the electron temperature in our experiment is much below the excitation threshold for autoionization. However, detailed theoretical calculations are necessary to estimate this contribution.

IV. CONCLUSION

The effective ionization rates of Ti IX, Ne VII, Ne VI, and O VI are determined experimentally using the plasma spectroscopy method at an electron temperature very much below threshold for ionization and at an electron density of a few times 10^{16} cm^{-3}. These rates are up to a factor of 2 higher than the total of ground-state and inner-shell ionization rates estimated by the Lotz-Kunze semiempirical formula. However, the addition of electron density-dependent contributions to the ionization rates from the low-lying and very-high-lying excited levels bring the effective theoretical rates close to the measurements.

ACKNOWLEDGMENTS

Many helpful discussions with Dr. H. R. Griem and Dr. S. M. Younger, constant encouragement of Dr. W. Wiese, and technical help of Tom Sellner are greatly appreciated. Dr. T. Pittman contributed immensely in the density measurements using the He-Ne—laser interferometer. This work is supported by the U. S. Department of Energy, Office of Fusion Energy, Contract No. EA-77-A-01-6010.

*Permanent address: University of Maryland, College Park, MD 20742.

[1]H.-J. Kunze, A. H. Gabriel, and Hans R. Griem, Phys. Rev. 165, 267 (1968).
[2]H.-J. Kunze, Phys. Rev. A 3, 937 (1971).
[3]R. U. Datla, L. J. Nugent, and Hans R. Griem, Phys. Rev. A 14, 979 (1976).
[4]E. Källne and L. A. Jones, J. Phys. B 10, 3637 (1977).
[5]W. L. Rowan and J. R. Roberts, Phys. Rev. A 19, 90 (1979).
[6]P. Greve, M. Kato, H.-J. Kunze, and R. S. Hornady, Phys. Rev. A 24, 429 (1981).
[7]L. A. Jones, E. Källne, and D. B. Thomson, J. Phys. B 10, 187 (1977).
[8]W. Lotz, Astrophys. J. Suppl. 14, 207 (1967); Report No. IPPI/62, Institut für Plasmaphysik, Garching bei München, 1967 (unpublished).
[9]A. W. Desilva and H.-J. Kunze, J. Appl. Phys. 39, 2458 (1968).
[10]R. J. Commisso and H. R. Griem, Phys. Rev. Lett. 36, 1038 (1976).
[11]A. R. Jacobson and D. L. Call, Rev. Sci. Instrum. 49, 318 (1978).
[12]R. U. Datla, University of Maryland Technical Report No. 76-104 (unpublished).
[13]S. M. Younger, Phys. Rev. A 22, 111 (1980).
[14]S. M. Younger, Phys. Rev. A 24, 1278 (1981).
[15]D. H. Sampson and L. B. Golden, J. Phys. B 11, 541 (1978).
[16]D. L. Moores, L. B. Golden, and D. H. Sampson, J. Phys. B 13, 385 (1980).
[17]H. P. Summers, Mon. Not. R. Astron. Soc. 169, 663 (1974); Internal Memo No. 367, Appleton Lab., England, 1974 (unpublished).
[18]A. Burgess, Culham Laboratory (Atomic Energy Research Es-

tablishment) Report No. 4818, 63 (1964) (unpublished).
[19]W. Lotz, Z. Phys. 216, 241 (1968).
[20]H. R. Griem, *Plasma Spectroscopy* (McGraw-Hill, New York, 1964).
[21]D. H. Crandall, R. A. Phaneuf, B. E. Hasselquist, and D. C. Gregory, J. Phys. B 12, L249 (1979); Oak Ridge National Laboratory Report No. ORNL-TM-7020 (unpublished).
[22]D. H. Crandall, R. A. Phaneuf, R. A. Falk, D. S. Belic, and G. H. Dunn, Phys. Rev. A 25, 143 (1982).

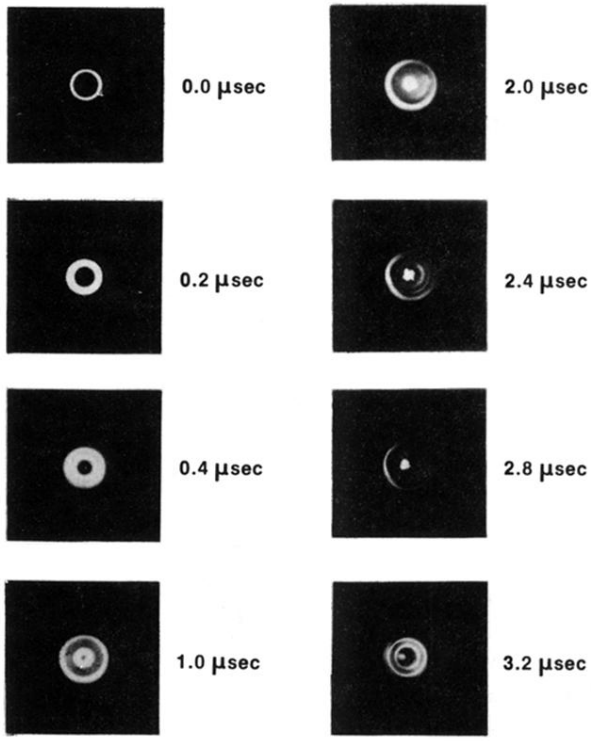

FIG. 1. End-on framing pictures of the θ pinch plasma. Time delay of each frame from the initiation of the main bank discharge is stated. Each frame is of 100-nsec duration.